American Mineralogist, Volume 77, pages 284–295, 1992

The calibration and application of accurate redox sensors

JEFF R. TAYLOR,* VIC J. WALL,** MARK I. POWNCEBY†
Earth Sciences Department, Monash University, Clayton 3168, Victoria, Australia

ABSTRACT

A new, solid H-sensor technique has been developed to monitor redox conditions during geologic experiments at elevated pressures and temperatures. The sensors are based upon previously calibrated O buffer equilibria [nickel–nickel oxide (NNO) or cobalt–cobalt oxide (CCO)] wherein the transition metal may be alloyed with Pd, or alternatively the oxide may form a continuous crystalline solution with MnO or MgO. The resultant lowering of the activity of the metal or metal oxide component displaces the equilibrium to more oxidizing or reducing conditions, respectively. For example, in the presence of their metallic components and H_2O, $(Ni_xMn_{1-x})O$ and $(Co_xMg_{1-x})O$ binary oxides can survey f_{O_2} more reduced than the pure NNO and CCO buffers. Alternatively, in the presence of their metal oxide component, Ni_xPd_{1-x} and Co_xPd_{1-x} alloys appraise conditions more oxidized than the pure NNO and CCO buffers.

In experimental systems at fixed P and T and with H_2O as the only volatile, a small mass of sensor assemblage cannot buffer redox state but will instead respond to the ambient f_{H_2} by adjusting its ratio of metal to metal oxide. In this manner, f_{O_2} can be calculated directly from the sensor composition, P and T, enabling f_{O_2} to be monitored and indeed bracketed over a range of $\approx$7.0 log f_{O_2} units. Nickel- and cobalt-based sensors cover most of the range of geologically significant redox conditions. The current accuracy of the sensors is largely dependent on the reliability of activity-composition relations in the relevant binary systems. Experiments have demonstrated that for optimum conditions the redox sensors are sensitive to about $\pm$0.01 log f_{O_2} and reversible down to at least 700 °C.

INTRODUCTION

Experimental petrologists have long recognized the importance of redox conditions in influencing a broad range of crustal and mantle chemical processes involving solids, aqueous fluids, and melts. As a result, any experimental system designed to simulate natural conditions requires some form of internal f_{O_2} constraint.

For experimental systems at 1 atm total pressure, f_{O_2} can be controlled conveniently by the use of gaseous mixtures of (H_2 + CO_2) or (CO + CO_2) (e.g., Nafziger et al., 1971; Huebner, 1987). At higher total pressures, studies of redox sensitive equilibria are carried out using two fundamentally different experimental approaches. One approach is to buffer the f_{O_2} of a system by using a well-calibrated solid assemblage. The O buffer technique pioneered by Eugster (1957) uses isothermally and isobarically invariant redox equilibria [e.g., nickel–nickel oxide (NNO) or quartz-fayalite-magnetite (QFM)] for controlling O-bearing atmospheres. The experimental system is sealed in a noble-metal capsule permeable to H and placed within another capsule containing the solid buffer assemblage and H_2O. Membrane equilibrium establishes the quality of the f_{H_2} in the outer and inner capsules. Eugster and Skippen (1967) and Huebner (1971) present applications and extensions of this technique.

A limitation of the Eugster method is that at fixed P and T, f_{H_2} can only be controlled in discontinuous steps, corresponding to the f_{O_2} generated by any given buffer assemblage. Shaw (1963) devised a second approach whereby f_{H_2} is controlled directly, thus circumventing the solid-state buffer and enabling redox conditions that are not dependent on solid-gas equilibria. In this technique an H reservoir is connected to a mechanically supported, metallic osmotic membrane that is positioned inside an autoclave adjacent to an H-permeable experimental charge. H diffuses across the membrane into an autoclave at P and T and ultimately into the experimental charge. Recent modifications and extensions of the Shaw technique are detailed by Gunter et al. (1987).

For experiments in an apparatus with no form of redox constraint, in solid-buffered experimental systems, or even where an H-permeable membrane facility is available, it is advantageous to measure f_{H_2} independently. The Ag-AgCl-HCl f_{H_2} sensor (Frantz and Eugster, 1973; Chou and Eugster, 1976) was therefore developed to monitor

* Present address: Petrogenesis Pty. Ltd., 16 Toorac Road, Upwey 3158, Victoria, Australia.
** Present address: MIM Exploration Pty. Ltd., G.P.O. Box 1042, Brisbane, Queensland, Australia.
† Present address: Bayerisches Geoinstitut, Universität Bayreuth, Postfach 101251, D-8580, Bayreuth, Germany.

0003–004X/92/0304–0284$02.00

f_{O_2}. In this technique, the f_{O_2} imposed by an experimental system is recorded by the sensor as H diffuses through the sensor wall and changes the ratio of Ag/AgCl and thereby the pH of the sensor's fluid phase. The pH measured on quench provides a measure of the f_{H_2}, which at any given P and T can be directly related to f_{O_2}. Applications of the H-sensor technique have been discussed by Chou and Eugster (1976) and Wood et al. (1975).

The tremendous potential of the H-sensor technique suffers from numerous possible uncertainties such as (1) determination of the dissociation constant for HCl as a function of P and T, (2) evaporation of fluid during extraction and analysis with a pH electrode, (3) sample dilution errors, and (4) errors associated with calibration of the electrode for salt effects. Additionally, the applicability of this technique at $P > 8$ kbar and $T > 800$ °C remains to be demonstrated. The complex microchemical analyses required and the numerous experimental uncertainties have discouraged many experimentalists from adopting the technique; hence many of the potential applications remain either unfinished or untested. Clearly what is needed is a simple, accurate means of determining redox conditions in high-temperature and high-pressure experimental systems. This paper discusses the systematics, calibration, and applications of H-sensitive binary compounds.

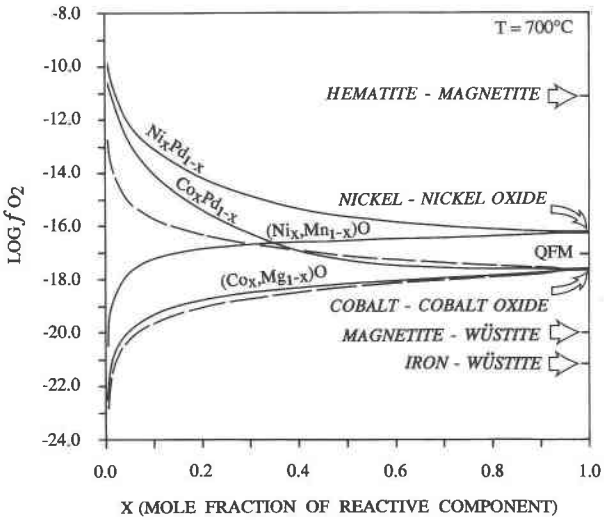

Fig. 1. Binary sensor systems at 700 °C. Solid lines are constructed from equations in Table 1. Dashed lines indicate results predicted assuming ideal mixing.

Theoretical

Thermodynamic considerations

The redox sensors are based on previously calibrated metal–metal oxide (MMO) buffer equilibria for which a generalized mass-action relation can be written as

$$xM + \frac{y}{2}O_2 = M_xO_y. \quad (1)$$

At a specified P and T, the equilibrium constant of Equation 1 may be expressed as

$$\log K_{(T,P)} = \log(a_{M_xO_y}) - \left[x \log(a_M) + \frac{y}{2}\log(f_{O_2})\right] \quad (2)$$

where M is the metallic element, x and y are stoichiometric coefficients, $K_{(T,P)}$ is the equilibrium constant at the tempurature and pressure of interest, a is the activity of the species i, and f_{O_2} is the oxygen fugacity. For pure phases, $a_{(M)}$ and $a_{(M_xO_y)}$ are equal to unity; hence,

$$\log K_{(T,P)} = -\frac{y}{2}\log(f_{O_2}). \quad (3)$$

Equation 3, of course, forms the basis for calculating the ambient f_{O_2} present when using the various solid-solid buffer equilibria of Eugster (1957).

If however the activity of the metal oxide component is lowered by dilution with another stable divalent metal oxide component (i.e., for Eqs. 1–3, $Y = 1$), the effect of $a_{M_xO} < 1.0$ on the f_{O_2} imposed can be calculated using

$$\log(f_{O_2}) = -2[\log K_{(T,P)} - \log(a_{M_xO})]. \quad (4)$$

Thus the effect of adding an additional metal oxide component to the system is to displace the end-member buffer reaction to lower f_{O_2} at any given temperature and pressure. Alternatively, dilution of the metal component with another suitable metal that displays a continuous and ideal solid-solution series (binary alloy) displaces the end-member buffer equilibria to higher f_{O_2} at any given temperature and pressure:

$$\log(f_{O_2}) = -2[\log K_{(T,P)} + \log(a_{M_x})]. \quad (5)$$

Using Equations 4 and 5 for the cobalt–cobalt oxide (CCO) and NNO buffers at 700 °C, the mole fraction of reactive component (X) is plotted as a function of f_{O_2} (represented by dashed curves in Fig. 1). Dashed curves are calculated assuming ideal mixing of reacting components (i.e., $a = X$).

Ostensibly, the addition of a diluent to one of the components of the MMO buffer has the effect of changing the f_{O_2} indicated in Equations 4 and 5. In practice however a Δf_{H_2} across the walls of a sensor capsule (established by an external buffer, an H membrane, or the experimental apparatus itself) will cause the small mass of sensor material to adjust its composition in order to approach equilibrium with the imposed atmosphere. Hence, taking the NNO system containing a fixed mass of metallic diluent, for example, a compositional readjustment to more oxidized conditions involves the conversion of nickel metal to nickel oxide. This reaction changes the mole fraction of both components of the binary alloy. The inherently self-adjusting capacity of small masses of the sensor mixtures in experimental systems permits their utility as sliding f_{H_2} sensors (cf. first usage of a similar term by Barton and Skinner, 1967, cited in Huebner, 1971).

Criteria for use as H sensor

No binary systems yet studied involving Ni, Co, or their respective oxides as a component behave truly ideally in the temperature range under consideration. Suitable diluents must therefore produce binary systems that satisfy the following criteria:

1. A continuous solid-solution series must form at elevated temperatures over the range in which it will be used. In addition, for the oxide systems, maximum differences in the ΔG_f^0 between oxide end-members is necessary to ensure that the diluent will be stable within a range of f_{O_2} where the other oxide will reversibly decompose. The same applies to the binary alloy systems. Metal diluents must be chosen so that equilibria with their monoxides occur at more reducing conditions than for the buffers.
2. Well-established activity-composition relations must be available in the temperature range of interest.
3. The oxide phase(s) must be essentially insoluble in the metal phase(s) and vice versa.

If we are able to satisfy these requirements, the binary solid solutions will respond to an imposed f_{H_2} using sliding compositional readjustments. Thus at fixed P and T and with pure H_2O as the fluid phase, f_{O_2} can be monitored and its equilibrium value calculated from the precise composition of the redox-sensitive solid solutions. Ambient f_{O_2} conditions may in fact be bracketed by two separate sensor capsules containing convergent solid-solution compositions.

Experimental background

Carapezza (1966) was the first experimental petrologist to use the binary solid solutions, albeit in a limited capacity. He developed a method for establishing continuously variable control of f_{O_2} at high pressures by diluting an NNO buffer assemblage with MgO. Unfortunately he failed to recognize the self-adjusting capacity of the mixtures and also took no account of potential problems arising from charge-capsule alloying (see discussion below). Since this initial study, the thermodynamic relations in the (Ni,Mg)O system and numerous other binary oxide and binary alloy solutions have been determined. These studies provide the necessary data to design solid, sliding H sensors capable of accurately recording experimental redox conditions over a broad range.

Binary oxides

The following binary oxide systems were considered most suitable for use as O sensors: $(Ni_xMn_{1-x})O$, $(Ni_xMg_{1-x})O$, and $(Co_xMg_{1-x})O$. All the end-member metal monoxides have the rocksalt structure, and their mixtures form continuous binary solid-solution series.

$(Ni_xMn_{1-x})O$. Thermodynamic properties of the NiO-MnO system have been studied extensively from 600 to 1300 °C using both gas equilibration and solid electrolyte galvanic cell (EMF) techniques. All the studies indicate small positive deviations from ideal mixing; however no consistent magnitude has been established. The most recent thermodynamic assessment (Bergman and Ågren, 1985) provides a comprehensive critical examination and recalculation of the available data. This study attributes much of the inconsistency among the earlier results to assumptions made during X-ray analysis of experimental products. Influenced by Barret and Evans (1964), who claimed that the system displayed significant deviation from Vegard's law, they chose to accept the activity data of Paulsson and Rosén (1977) and Labus and Rog (1975). We concur with the conclusions of Bergman and Ågren and accept their algorithm for the calculation of high-temperature, solid-state activity data. This activity-composition data set is the only one that is directly obtainable from a polynomial expression, contains temperature dependant terms, and has been specifically determined in the temperature range of interest to the present study.

$(Ni_xMg_{1-x})O$. Three controlled-atmosphere equilibration studies in the NiO-MgO system by Hahn and Muan (1961, 1970) and Evans and Muan (1971) are available. The first two indicate near ideal mixing at 1100–1300 °C; the latter study suggests minor negative deviations from ideal mixing at 1400 °C. Paulsson (1982) attempted to reconcile these differences by studying a narrow compositional range using a solid state EMF technique. He concluded that the system displays small positive deviations from ideality but may be classified as near ideal. The temperature dependence of the mixtures between 1000 and 1450 K is within the limits of experimental uncertainty. Activity-composition data from this study were chosen for use here.

$(Co_xMg_{1-x})O$. Early controlled-atmosphere equilibration studies indicate ideal mixing in the CoO-MgO system (Aukrust and Muan, 1963; Brezny and Muan, 1971). More recent work using solid-state galvanic cells shows small positive deviations from ideality. The first of these, by Seetharaman and Abraham (1971), indicated conformity of the system to a regular solution model. Riguad et al. (1974) repeated the study claiming that erratic cell behavior in the former study compromised the quality of the results. Small but experimentally significant variations from the reported activity-composition relations were proposed, and the study indicated that the system does not conform to a regular solution model. The most recent EMF work by Torkar and Inselbacher (1980) at temperatures between 1100 and 1300 K is in good agreement with the earlier study by Seetharaman and Abraham. They report the solution is regular and confirm the small deviation from ideality. Activity coefficients from this latest study are used here.

Binary alloys

Pd and Pt were both considered to be suitable additives for the formation of Ni- or Co-bearing binary alloys. The former was chosen primarily to overcome the numerous phase transformations in Pt-bearing alloys at low to intermediate temperatures (Massalski, 1986). The lower cost of Pd as opposed to Pt was an additional incentive.

TABLE 1. Calibration expressions for H sensors

$$\log f_{O_2}(Ni,Mn)O = 2\log X_{NiO} - 1/(2.3025\,RT)\{(480104 - 244.700T + 21.1078T\log T) - [2(1 - X_{NiO})^2(9731 + 2.388T)]\} \quad [873 \le T(K) \le 1573]$$

$$\log f_{O_2}(Ni,Mg)O = 2\log X_{NiO} - 1/(2.3025\,RT)\{(480104 - 244.700T + 21.1078T\log T) - [2(1 - X_{NiO})^2(0.693 + 512.0(6X_{NiO} - 1)(2X_{NiO} - 1)]\}$$
$$[1000 \le T(K) \le 1450]$$

$$\log f_{O_2}(Ni,Pd) = -2\log X_{Ni} - 1/(2.3025\,RT)\langle(480104 - 244.700T + 21.1078T\log T) + \{2(1 - X_{Ni})^2[-8.93T + 7647(4X_{Ni} - 1)]\}\rangle$$
$$[973 \le T(K) \le 1473]$$

$$\log f_{O_2}(Co,Mg)O = 2\log X_{CoO} - 1/(2.3025\,RT)\{(491649 - 508.527T + 122.6909T\log T - 0.02518T^2) - [2(1 - X_{CoO})^2(2140 + 2.10T)]\}$$
$$[1100 \le T(K) \le 1300]$$

$$\log f_{O_2}(Co,Pd) = -2\log X_{Co} - 1/(2.3025\,RT)\langle(491649 - 508.527T + 122.6909T\log T - 0.02518T^2) + \{2(1 - X_{Co})^2[-9.76T + 16445(4X_{Co} - 1)]\}\rangle \quad [973 \le T(K) \le 1473]$$

Note: Operational temperature limits indicated.

Ni_xPd_{1-x} and Co_xPd_{1-x} binary alloys each form a continuous solid solution between 500 °C and the melting temperature (1237 °C for $Ni_{45}Pd_{55}$ and 1219 °C for $Co_{48}Pd_{52}$: Wise, 1968; Hultgren et al., 1973; Massalski, 1986). Activity-composition data for Ni_xPd_{1-x} and Co_xPd_{1-x} alloys were extracted from Bidwell and Speiser (1965) and Schwerdtfeger and Muan (1965). The former workers used an EMF cell at 700 to 1200 °C for the Ni alloys, and the latter employed both EMF determination and controlled-atmosphere equilibrium studies at 1000 and 1200 °C for both alloy systems. Bidwell and Speiser (1965) concluded that Ni-rich alloys display positive departures from Raoult's law for the solvent and negative deviations for the solute, whereas Pd-rich solutions exhibit negative deviations for both the solvent and solute. Similar conclusions were drawn by Schwerdtfeger and Muan (1965) for both the Ni- and Co-bearing Pd alloys. In addition, a pronounced temperature effect on the behavior of Co-rich Co_xPd_{1-x} alloys ($X_{Co} > 0.5$) was noted, and a miscibility gap was considered likely below 1000 °C. Because of its extensive temperature range and internal consistency, the work of Bidwell and Speiser for Ni_xPd_{1-x} alloys was given precedence (cf. Meschter, 1981). The data of Schwerdtfeger and Muan (1965) were used for the Co_xPd_{1-x} alloy system.

One of the authors (M.I.P.) is currently recalibrating the Ni_xPd_{1-x} and Co_xPd_{1-x} systems over the temperature range 600–1000 °C using an accurate electrochemical technique with O-specific CSZ electrolytes.

CALIBRATION

Calibration curves relating sensor composition and f_{O_2} were constructed from simple relationships of the form indicated by Equations 4 and 5. Activity coefficients for the binary oxide and alloy systems were taken from the preferred aforementioned studies and fitted to a polynomial of the Redlich-Kister form

$$\log \gamma = \left(\frac{1}{2.303}RT\right)(1 - X)^2 \cdot [(C1 + C2T) + (C3 + C4T)(4X - 1) \cdot (C5 + C6T)(6X - 1)(2X - 1) \cdot (C7 + C8T)(8X - 1)(2X - 1)(2X - 1)] \quad (6)$$

where γ is the activity coefficient of the solvent species, X its mole fraction, T the temperature in degrees kelvin, R the universal gas constant, and C1 to C8 are regression coefficients. Equilibrium constants, $K_{(T,P)}$, for the NNO and CCO buffers were obtained from recent O chemical-potential calibrations by O'Neill (1987b).

For the binary systems, substituting the relevant R-K polynomial and the appropriate $K_{(T,P)}$ algorithm into Equations 4 or 5 enables immediate interpolation of f_{O_2} for any given sensor composition over a range of temperatures. The expressions derived for each of the sensor systems are given in Table 1.

Depicted in $\log f_{O_2}$-X (mole fraction of reactive component) space at 700 °C, the four operating sensor systems are represented by the solid exponential curves in Figure 1. Two additional curves (dashed lines) displaying ideal dilution of both the oxide and metallic components of the CCO buffer (see previous discussion) and the location of several other redox buffers are included for reference. From the curves in Figure 1 it is clear that as the mole fraction of the reactive species approaches zero, the attendant f_{O_2} approaches an infinitely small value in the binary oxide sensors and an infinitely large value for the binary alloys. Ni_xPd_{1-x} alloys extend the sensors to their most oxidized extremities [within the influence of the hematite-magnetite buffer (HM)], and $(Co_x$-$Mg_{1-x})O$ oxides can record f_{O_2} as reduced as the iron-wüstite buffer (IW). The sensors therefore provide a means of accurately recording experimental f_{O_2} values over an effective working range of $\approx$7.0 log units.

Comparison of the calculated sensor curves with the model predicted assuming ideal mixing illustrates the importance of accurate activity-composition data for all systems. Although regular solutions displaying the smallest deviations from ideality introduce the smallest errors, negative deviations from ideal mixing for NiO and CoO components of the binary oxides and positive deviations for the Ni and Co-metal components of the binary alloys enhance the resolution of the O monitors over the entire range of compositions. In fact, the larger the departure from ideal mixing for any of the binary solid solutions, the broader the range of f_{O_2} able to be recorded.

EXPERIMENTAL STRATEGY

Binary oxide sensors are composed of fixed proportions of the two metal monoxide components and an excess of the metallic component. It is possible to oxidize

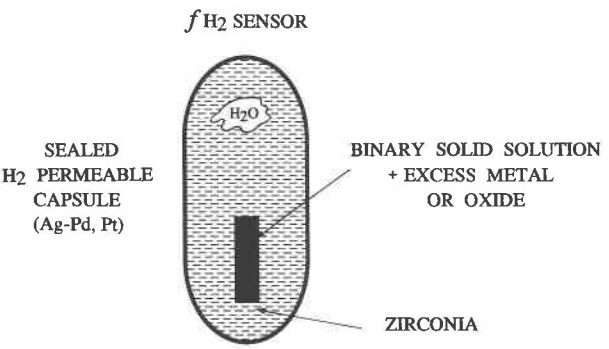

Fig. 2. Schematic diagram showing experimental arrangement of the H-sensor technique.

the reactive metal component by subjecting the sensor assemblage to oxidizing conditions. In contrast, any binary oxide sensor exposed to more reducing conditions cannot exhaust its reactive oxide constituent. It can however reduce its proportion to diminishingly small quantities, well beyond analytical detection limits. Hence the proportion of metallic constituent added to a binary oxide mixture will depend on the direction and degree of compositional shift expected for a given application. Binary alloy sensor systems are composed of fixed proportions of the two metallic components and an excess of the appropriate metal-monoxide. Although it is not possible to exhaust the metal oxide component in binary alloy systems if the sensor mixture is exposed to more oxidizing conditions, a more reducing atmosphere may result in its complete consumption.

These features of the redox sensors are a function of the exponential nature of the f_{O_2}-X (mole fraction of reactive component) curves depicted in Figure 1. For many applications, such a property is conceivably advantageous. The choice of a sensor composition with a mole fraction of reactive component set close to unity has the ultimate sliding capacity (compositional mobility). In practical terms, however, the proportion of solid solution available for analysis in the sensor mixture will diminish with the degree of slide.

For any sensor composition, a progression to relatively oxidizing conditions will also result in the consumption of H_2O. Thus, care should be taken to provide sufficient H_2O to enable conversion of the reactive metal component to its monoxide. For the systems studied here, 1 mole of H_2O is required to convert 1 mol of Ni or Co metal to 1 mol of its respective monoxide.

Normally, the systematics of any binary solid solution will determine the operational temperature range of the associated sensor mixtures. The upper limits are generally controlled by the solidus surface of the metals or alloys, whereas lower limits can be a function of the formation of discrete immiscible phases (unmixing), the minimum temperatures of the available thermodynamic data, or the lowest temperature at which H permeates noble-metal capsules.

Preparation

Starting materials were prepared from finely ground (<50 μm) analytical reagents. Co, CoO, Ni, NiO, and Pd (black) were oven dried at 110 °C for 24 h. MgO was fired at 1200 °C for 24 h, and MnO was prepared by firing $MnCO_3$ at 800 °C for 5 h in a reducing environment. All materials were X-rayed to confirm their stoichiometry and stored under vacuum until used.

Solid solutions chosen to provide experimental reversals were mixed and ground by hand under acetone in an agate mortar and pestle. Mixtures were transferred to a tungsten-carbide mill for further pulverization and homogenization. Grain mounts of the final mixtures were made to confirm a uniform grain size of <5 μm. Mixtures were fabricated into cylindrical pellets 2–3 mm long and 2.3 mm od in a manually operated stainless steel press. These were oven dried and desiccated ready for use.

To ensure rapid equilibration of the solid solutions with the imposed H pressure, AgPd alloys and thin-walled Au were chosen as the encapsulating material. The charges were constructed from 25-mm lengths of 5.0-mm od × 4.6-mm id AgPd (70:30 or 50:50) or Au tubing. The tube was triple crimped and arc welded at one end. Since Ni and Co metal readily form alloys with the components of the commonly used H-permeable noble-metal capsules (Au, Ag, Pd, and Pt), the redox sensitive mixtures have to be isolated from the capsule walls to minimize mass transfer. Inert ZrO_2 jackets were designed for this purpose (refer to Fig. 2). An appropriate quantity of very fine-grained ($\approx$1 μm) analytical reagent ZrO_2 powder was deposited into the capsule. A small cylindrical hole within the powder, designed to accommodate the sensor, was fabricated in one of two ways: (1) dry ZrO_2 powder was compressed with a stainless steel die of the required shape, or (2) 2–3 drops of H_2O were added to the capsule to produce a thick ZrO_2 slurry. A solid stainless steel rod was inserted into the center of the mixture. The entire assembly was oven dried, and the rod was carefully extracted.

Prefabricated crushable jackets (Ceramic Oxide Fabricators, Eaglehawk, Victoria, Australia) used in the latest experiments simplified sample preparation even further.

A further small quantity of ZrO_2 was added to the charge to ensure that the base of the hole was completely remote from the capsule margins. The prefabricated pellet of sensor was lowered into the ZrO_2 mold and the exposed portion of the sensor covered with more ZrO_2. Approximately 12.5 μL H_2O were added, and the charge was finally triple crimped and arc welded closed. Note that on loading the sensor charges, account should be taken of the specific volume of H_2O under experimental conditions. As long as the volume of the H_2O at P and T is significantly less than the volume available in the capsule, the confining pressure will maintain the physical integrity of the ZrO_2 jacket. This is essential for trouble-free operation of the redox sensors. As an added precaution to ensure that the ZrO_2 jacket remained intact during the ex-

periment, the body of the charge was crimped flat down to the sensor assembly.

Operation

Experiments were conducted at 700, 750, and 800 °C and 2.0 kbar within a large-volume, internally heated pressure vessel fitted with an H osmotic membrane. Temperatures were achieved by dual-element Inconel-sheathed resistance furnaces. Three stepped chrome-alumel thermocouples, calibrated against a Pt-$Pt_{90}Rh_{10}$ standard thermocouple provided by the National Measurement Laboratory (Australia), enabled temperatures to be measured within ±2 °C. Manganin cells calibrated against a Bourdon Heise gauge permitted Ar confining pressures to be established to ±20 bars. A factory calibrated 3000 psi full-scale Heise gauge permitted H pressure to be recorded with a precision of ±1 psi. The semipermeable H membrane consisted of a $Ag_{40}Pd_{60}$ tube, 5.0-mm od × 4.6-mm id, filled with a solid, sintered alumina rod. To facilitate gas equilibration across the membrane, a quantity of H was introduced to the pressure vessel prior to activating the furnaces. Thus the differential H_2 pressure across the membrane was minimized and the vessel-sample H equilibration time dramatically reduced. Experiment duration times varied between 46 and 280 h.

On completion of the experiments, the capsules were weighed, punctured, and then oven dried. Capsules were then reweighed to confirm that H_2O remained during experimentation. Capsules displaying no weight change after drying were discarded.

Zirconia pellets were almost invariably removed from the capsules completely intact. They appeared as pure white, irregularly shaped oblate ellipsoids. Rare instances where visible solid-solution material had breached the jacket margins during loading were discarded immediately because of the likelihood of mass transfer between the sensor mixture and the capsule. The slugs of ZrO_2 were dense and hard, and they required dissection with a metallic cutting tool in order to expose the core of solid-solution material. All sensor compositions were extracted as coherently sintered pellets except for the $(Co_xMg_{1-x})O$ oxides, which maintained a disaggregated powder form. The oxide mixtures produced anhedral, fine-grained (≈20 μm) material, whereas the alloys developed coarse-grained, homogeneous lobate and circular blebs of metal (≈200 μm). $(Ni_xMn_{1-x})O$ and $(Ni_xMg_{1-x})O$ oxides appeared as various shades of lime green and dark green, respectively, whereas $(Co_xMg_{1-x})O$ mixtures were dark brown in color.

Analysis

Solid solutions were mounted in epoxy resin and analyzed by wavelength dispersive analysis on an ARL SEMQ-II microprobe. Accelerating voltages of 20–25 kV and beam currents of between 20 and 30 nA were employed, with an average of 10–15 analytical points per sample. Standards were the pure metals for Ni, Pd, and Co; synthetic pyrophanite ($MnTiO_3$) crystals for Mn; and a stoichiometric diopside for Mg. Backscattered and secondary electron images were used in conjunction with X-ray mapping to facilitate the analytical work.

Table 2 documents the experimental conditions and results of all the f_{H_2} sensor studies. The analytical data recovered from these experiments are subject to normal analytical errors as well as relatively large uncertainties arising from logistical experimental constraints. The sensors were initially designed to monitor the redox conditions in a series of trace-element partitioning and solubility studies (Taylor, 1988) and consequently were accommodated in whatever space remained in the sample holder after the principal charges had been loaded. This meant that the distribution of sensors relative to minor thermal gradients along the chamber was not well established. Furthermore, pairs of sensors could not be juxtaposed, which would have confirmed that any given sensor composition was responding under essentially isothermal conditions to the imposed f_{H_2}. For both the NNO and CCO buffer systems, a gradient of 10 °C accounts for ≈0.25 log units shift in the attendant equilibrium f_{O_2} at temperatures in the vicinity of 700 °C. It is evident that even small thermal gradients, either within or between charges, can have a substantial effect on the sensor composition, especially for mixtures with high mole fractions of reactive component.

Although the electron microprobe is capable of resolving down to 0.1 mol%, internal heterogeneity within the large mass (30–50 mg) of sensor used in these experiments, probably partly because of small temperature gradients within the sensor charges, reduces the accuracy to 0.3–0.8 mol%. The error arising from this analytical variability was calculated by the method outlined in Seifert and O'Neill (1987) and combined with the much larger potential error arising from the maximum possible thermal gradients between sensor charges.

The results presented in Table 2 will also be a function of the reliability of activity-composition data in the relevant binary solution systems. No thorough appraisal has been attempted of the error brackets on the activity-composition data, but they are expected to be significantly smaller than the error limits quoted in Table 2 (refer to later discussion).

Results and discussion

It was evident after a few experiments that the $(Ni_xMg_{1-x})O$ system was not suited to the relatively low temperatures and short experiment durations of the present investigation. No consistent analyses could be extracted from any of the samples, with large and often unpredictable variations in composition occurring on a small scale. The most Ni-rich compositions were most commonly found proximal to small blebs of metallic Ni, indicating a relatively sluggish equilibration rate in this system. No useful f_{O_2} measurements were obtained from $(Ni_xMg_{1-x})O$ oxides.

The remaining solid-solution systems responded to the

TABLE 2. Summary of experimental results using redox sensors

Exp no.	Charge no.	Capsule material	Time (h)	T (°C)	P (H_2) (psi)*	Sensor system	Composition** Initial (x)	Composition** Final (x)	log f_{O_2} Imposed	log f_{O_2} Calculated	Max. error†
2014	C	$Ag_{(70)}Pd_{(30)}$	106	750	360	$[Ni_{(x)},Mn_{(1-x)}]O$	0.25	0.088	−15.98	−16.12	±0.044
	D	$Ag_{(70)}Pd_{(30)}$				$[Ni_{(x)},Mn_{(1-x)}]O$	0.45	0.079		−16.20	±0.039
1050	C	Au	46	750	1500‡	$[Ni_{(x)},Mn_{(1-x)}]O$	0.28	0.129	?	−15.88	±0.140
	T	$Ag_{(70)}Pd_{(30)}$				$[Ni_{(x)},Mn_{(1-x)}]O$	0.04	0.048		−16.56	±0.136
1051	K	Au	92	800	?‡	$Ni_{(x)},Pd_{(1-x)}$	0.30	0.367	?	−12.82	±0.144
	S	Au				$Ni_{(x)},Pd_{(1-x)}$	0.80	0.729		−13.69	±0.145
1052	M	Au	170	750	64	$Ni_{(x)},Pd_{(1-x)}$	0.30	0.426	−14.47	−14.18	±0.099
2033	O	Au	183	800	80	$Ni_{(x)},Pd_{(1-x)}$	0.30	0.356	−13.42	−12.78	±0.148
	W	Au				$Ni_{(x)},Pd_{(1-x)}$	0.80	0.700		−13.65	±0.145
2034	J	$Ag_{(50)}Pd_{(50)}$	99	800	392	$[Ni_{(x)},Mn_{(1-x)}]O$	0.20	0.160	−14.84	−14.68	±0.086
	I	$Ag_{(50)}Pd_{(50)}$				$[Ni_{(x)},Mn_{(1-x)}]O$	0.50	0.166		−14.66	±0.085
1055	A17	$Ag_{(50)}Pd_{(50)}$	158	800	1230	$[Ni_{(x)},Mn_{(1-x)}]O$	0.04	0.068	−15.81	−15.22	±0.037
	A18	$Ag_{(50)}Pd_{(50)}$				$[Ni_{(x)},Mn_{(1-x)}]O$	0.28	0.067		−15.23	±0.036
	A15	$Ag_{(50)}Pd_{(50)}$				$[Co_{(x)},Mg_{(1-x)}]O$	0.15	Exhd.		—	—
	A16	$Ag_{(50)}Pd_{(50)}$				$[Co_{(x)},Mg_{(1-x)}]O$	0.70	0.850		−15.51	±0.041
1056	R	$Ag_{(50)}Pd_{(50)}$	161	750	357	$[Ni_{(x)},Mn_{(1-x)}]O$	0.20	0.196	−15.99	−15.66	±0.072
	L	$Ag_{(50)}Pd_{(50)}$				$[Ni_{(x)},Mn_{(1-x)}]O$	0.50	0.187		−15.68	±0.074
	A19	$Ag_{(50)}Pd_{(50)}$				$Co_{(x)},Pd_{(1-x)}$	0.35	0.435		−15.83	±0.060
	D1	$Ag_{(50)}Pd_{(50)}$				$Co_{(x)},Pd_{(1-x)}$	0.75	0.440		−15.85	±0.062
2036	1	$Ag_{(50)}Pd_{(50)}$	69	800	391	$[Ni_{(x)},Mn_{(1-x)}]O$	0.04	Exhd.	−14.80	—	—
	3	$Ag_{(50)}Pd_{(50)}$				$[Ni_{(x)},Mn_{(1-x)}]O$	0.50	0.559		−14.20	±0.098
	4	$Ag_{(50)}Pd_{(50)}$				$[Ni_{(x)},Mn_{(1-x)}]O$	0.20	0.553		−14.20	±0.096
2037	D8	$Ag_{(50)}Pd_{(50)}$	75	800	1650	$[Ni_{(x)},Mn_{(1-x)}]O$	0.20	0.070	−16.05	−15.20	±0.133
	D10	$Ag_{(50)}Pd_{(50)}$				$[Ni_{(x)},Mn_{(1-x)}]O$	0.50	0.070		−15.20	±0.129
	A22	$Ag_{(50)}Pd_{(50)}$				$Co_{(x)},Pd_{(1-x)}$	0.35	Exhd.		—	—
	D4	$Ag_{(50)}Pd_{(50)}$				$Co_{(x)},Pd_{(1-x)}$	0.75	Exhd.		—	—
2038	6	$Ag_{(50)}Pd_{(50)}$	140	800	45	$Ni_{(x)},Pd_{(1-x)}$	0.30	0.388	−12.92	−12.91	±0.156
	5	$Ag_{(50)}Pd_{(50)}$				$Ni_{(x)},Pd_{(1-x)}$	0.80	0.412		−13.00	±0.152
	A23	$Ag_{(50)}Pd_{(50)}$				$Co_{(x)},Pd_{(1-x)}$	0.35	0.222		−13.35	±0.153
	D5	$Ag_{(50)}Pd_{(50)}$				$Co_{(x)},Pd_{(1-x)}$	0.10	0.250		−13.60	±0.156
2042	D7	$Ag_{(50)}Pd_{(50)}$	280	700	320	$[Ni_{(x)},Mn_{(1-x)}]O$	0.20	0.170	−17.26	−16.93	±0.108
	D9	$Ag_{(50)}Pd_{(50)}$				$[Ni_{(x)},Mn_{(1-x)}]O$	0.50	0.180		−16.90	±0.104
	A21	$Ag_{(50)}Pd_{(50)}$				$Co_{(x)},Pd_{(1-x)}$	0.35	0.440		−17.09	±0.107
	D3	$Ag_{(50)}Pd_{(50)}$				$Co_{(x)},Pd_{(1-x)}$	0.75	0.445		−17.10	±0.105
2044	Q	Au	211	700	42	$Ni_{(x)},Pd_{(1-x)}$	0.30	0.480	−15.47	−15.60	±0.071
	X	Au				$Ni_{(x)},Pd_{(1-x)}$	0.80	0.490		−15.63	±0.069
	A24	$Ag_{(50)}Pd_{(50)}$				$Co_{(x)},Pd_{(1-x)}$	0.35	0.223		−15.66	±0.066
	D6	$Ag_{(50)}Pd_{(50)}$				$Co_{(x)},Pd_{(1-x)}$	0.10	0.221		−15.64	±0.065

Note: All experiments conducted at $P = 2.0$ kbar. Exhd. = reactive component of solid solution exhausted.
* H pressure derived by averaging values during final phase of experiment.
** Mole fraction (x).
† Error calculation includes analytical variation and uncertainties introduced by the maximum thermal gradient within each experiment.
‡ Faulty membrane passing Ar; actual H pressure unknown.

ambient redox conditions within the experimental time frames at the temperatures examined. Reversal compositions readily converged on their equilibrium values, and in general the different sensor systems indicated remarkably consistent f_{O_2} (Table 2).

Poor reversals within some of the early experiments (1050, 1051, and 2033) are the result of their short duration and low H partial pressures for sensor mixtures encapsulated by Au, suggesting that H permeability through charge walls is the key rate-limiting step. Experiments 1050 and 1051 were terminated prematurely because of mechanical failure of the H membrane. Ar leaking into the H reservoir resulted in spuriously high H-pressure readings.

In AgPd capsules, approximately 70 h at 800 °C was sufficient to equilibrate binary oxide mixtures in the $(Ni_xMn_{1-x})O$ system with the imposed f_{H_2}. Although experiments of comparable duration have not been conducted with the two alloy systems, preliminary EMF results by one of us (M.I.P.) indicate that under anhydrous conditions equilibrium in the binary alloy systems can be established in less than 12 h at $T \geq 800$ °C. No formal rate-of-reaction tests were carried out during the study presented here.

Nonreversible exhaustion of one of the sensor components occurred four times during the investigation, primarily the result of poor choice of starting sensor composition. In addition, as a result of initially choosing the wrong activity-composition data for the $(Ni_xMn_{1-x})O$ system, all of the compositional brackets failed to reverse the imposed f_{O_2}. All, however, managed to approach essentially the same final sensor composition, thereby indicating equivalent f_{O_2}. A mechanically constricted H membrane in experiment 2014 also contributed to this problem. This accounts for the discrepancy between the imposed and calculated f_{O_2}. Fortuitously, sufficient H was introduced to the pressure vessel prior to operation to allow an on-scale f_{O_2} reading to be recorded, albeit different from the desired value.

Most of the experiments display a discrepancy between

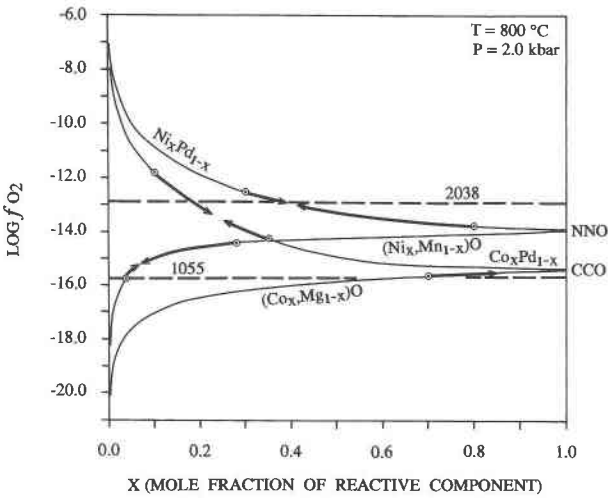

Fig. 3. Results from experiments 1055 and 2038 conducted at 800 °C. Circles indicate starting sensor composition; arrowheads the final sensor composition. Dashed lines represent the f_{O_2} set using the H membrane.

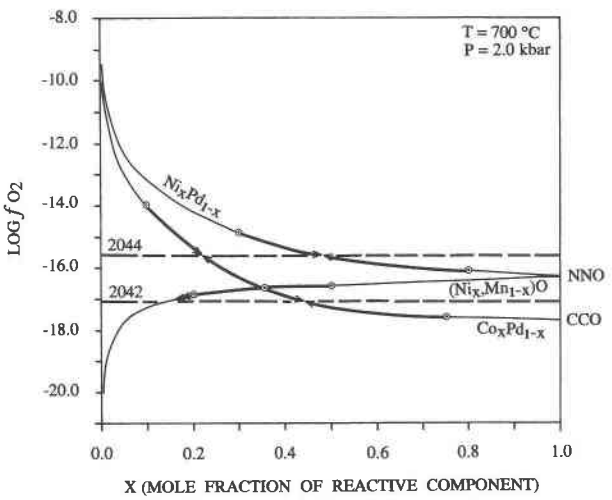

Fig. 4. Results from experiments 2042 and 2044 conducted at 700 °C. Symbols same as for Figure 3.

their imposed and calculated f_{O_2}, with the latter almost invariably being lower than the imposed value. The most reduced experiments (1055 and 2037) display the greatest variance. The comparatively high H pressures imposed during these experiments are most probably associated with the greatest Δf_{H_2} across the osmotic membrane. It is likely therefore that incomplete H equilibration across the membrane is responsible for much of the difference between the imposed and calculated f_{O_2} (i.e., short experimental durations). This reemphasizes that H diffusion through metallic membranes is the rate-limiting step in the application of the redox sensors.

Comparison between sensor systems—relative accuracy

The large errors quoted in Table 2 arising from the maximum possible thermal gradients within each experiment prohibit a thorough comparison between the sensor systems at a fixed P, T, and f_{H_2}. Figures 3–5 are graphical representations of experimental data at 800, 700, and 750 °C, respectively. These plots permit preliminary comparison of the activity-composition relations between different sensor systems. Despite the large error brackets, experiment 1055 (Fig. 3) demonstrates that at 800 °C, the $(Ni_xMn_{1-x})O$ solid solutions record more oxidized conditions than the $(Co_xMg_{1-x})O$ sensor system. Similarly, experiment 2038 (Fig. 3) confirmed that at 800 °C Ni_xPd_{1-x} alloys register more oxidized conditions than Co_xPd_{1-x} alloys.

At fixed T, P, and f_{H_2}, the disparity between sensor systems in the remaining data are all within the large error limits. Regardless of this, experiment 2044 at 700 °C (Fig. 4) supports the findings in experiment 2038 and infers that Ni_xPd_{1-x} alloys preserve slightly more oxidized conditions than Co_xPd_{1-x} alloys (see Table 2). In addition, Figure 4 suggests that at 700 °C, Co_xPd_{1-x} sensors indicate more reduced conditions than $(Ni_xMn_{1-x})O$ sensors. This is further supported by experiment 1056 at 750 °C (Fig. 5). The broad similarity of the calculated f_{O_2} values both within and between the different sensor systems at constant P, T, and f_{H_2} strongly suggests that the maximum possible errors listed in Table 2 are overestimates.

Comparison with solid buffers—absolute accuracy

Having confirmed the performance of the solid solutions as simple H monitors during the initial phase of this study, further experiments were designed to test the absolute accuracy of the activity-composition data. Four small sensors representing two reversed sensor systems were placed within a thick-walled, H-impermeable outer Ag charge containing a QFM mixture. To prolong the life

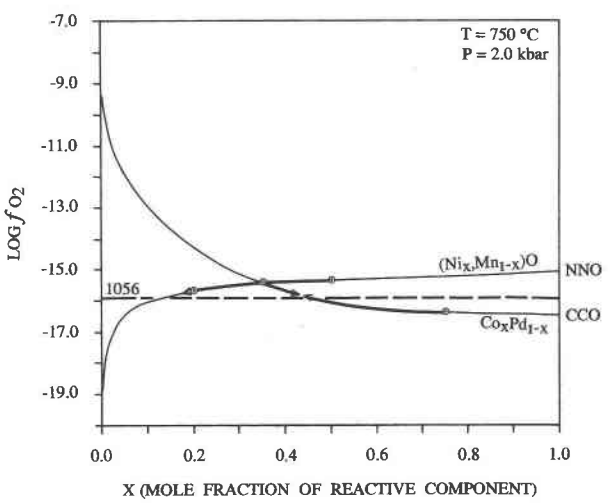

Fig. 5. Results from experiment 1056 conducted at 750 °C. Symbols same as for Figure 3.

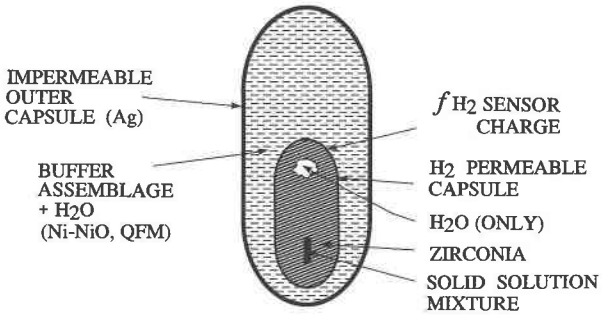

Fig. 6. Experimental design for examining the absolute accuracy of the redox sensors.

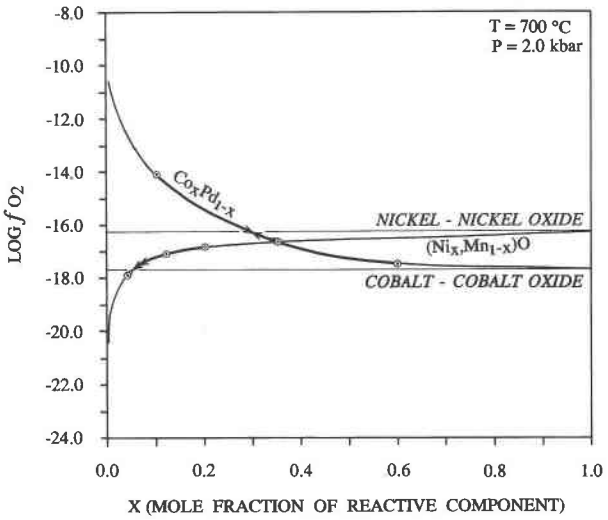

Fig. 7. Comparison of experimental reversals for the Co_xPd_{1-x} and $(Ni_xMn_{1-x})O$ sensor systems against NNO and CCO solid buffers. Circles indicate starting sensor composition; arrowheads, the final sensor composition. Solid lines are the preset f_{O_2} of the experimental vessel.

of the solid buffer components (in case of H diffusion through the capsule walls), an external pH_2 was set at 223 psi ($f_{O_2} = -16.75$ log units). Reversals were obtained at 700 °C and 2.0 kbar, with an experimental duration of 108 h. A diagrammatic representation of this procedure is shown in Figure 6. The proximity of the f_{O_2} calculated with the sensors to the recent determination of QFM by O'Neill (1987a) was considered a good measure of their accuracy. Similar experiments were conducted with the NNO and CCO buffers and compared with the results of O'Neill (1987b).

Results from the solid buffer experiments are given in Table 3 and represented graphically (except for the QFM experiment) in Figure 7. For the experiments using the NNO and CCO solid buffers, results indicate that the Co_xPd_{1-x} and $(Ni_xMn_{1-x})O$ sensor systems permit close prediction of f_{O_2}. Sensor compositions for the tightest reversals in each experiment display close convergence. Differences in the imposed and calculated f_{O_2} for each experiment were ≈0.03 log units.

Unfortunately the cross-calibration of both sensor systems against QFM was not entirely successful. All four sensors record a value for QFM more oxidizing (≈0.3–0.4 log units) than expected. This may be because H permeated the capsule walls and all sensors responded to the surrounding f_{H_2}, or alternatively the value we used for QFM at 700 °C is incorrect. Further work is needed to resolve this discrepancy. However, despite the "failure" of this experiment, it is worth noting that sensor composition of both types converged to within ≈0.07 log f_{O_2} units and within ≈0.09 log units of the externally imposed f_{H_2}.

Considering the errors inherent in the solid buffer calibrations (O'Neill, 1987a, 1987b) as well as the unknown error in the activity-composition relationships for the individual sensor systems, the results indicate that the calibration expressions in Table 1 enable close prediction of redox conditions. Interestingly, in each of the solid buffer experiments, the $(Ni_xMn_{1-x})O$ sensor system recorded more oxidizing conditions than expected, whereas the Co_xPd_{1-x} system recorded more reduced conditions. This was also evident in the earlier H membrane experiments discussed above. Clearly there is an error in the activity-composition relations for one or both sensor systems (albeit small); hence these systems will require accurate calibration and cross-calibration before their full potential may be realized.

The absolute accuracy of activity-composition relations in the additional two sensor systems [Ni_xPd_{1-x} and $(Co_xMg_{1-x})O$] were not checked during the course of this study. As a consequence, the validity of these binary solid-solution systems as accurate f_{H_2} monitors needs to be further explored. Results detailed in the previous section clearly illustrate the potential of these systems as indicators of redox state. However, the T limits for the current calibration expressions (Table 1) for $(Co_xMg_{1-x})O$ lie outside the range of temperatures used in these experiments. A recalibration of both Ni_xPd_{1-x} and $(Co_xMg_{1-x})O$, as well as a cross-calibration against solid f_{O_2} buffers, is likely to be necessary before they are used as highly accurate redox sensors.

Applications of sensors

Measurement of f_{H_2} (or temperature) in pressure vessels

Recent work into the effects of H on phase relations in silicate systems has identified new phenomena that have classically been considered to be unaffected by oxidation state. Luth and Boettcher (1986) have quantified the influence of f_{H_2} and f_{O_2} on the fluid-present solidi of albite, diopside, and quartz. They concluded that the dissolution of H in these silicate liquids inhibits the solution of H_2O and thereby increases the solidus temperature of each system. Additionally, high T and P rock mechanics experiments have recognized the significance of f_{O_2} on the hy-

TABLE 3. Experiments using solid buffers

Capsule	Sensor system	Sensor composition		log f_{O_2}		
		Initial	Final	Calculated	Imposed	Δ log f_{O_2}
1061 2	$Co_{(x)}Pd_{(1-x)}$	0.35	0.2978 ± 0.0005	−16.31	−16.28	−0.03
1061 3	$Co_{(x)}Pd_{(1-x)}$	0.10	0.2951 ± 0.0003	−16.29	(NNO)	−0.01
1061 9	$Co_{(x)}Pd_{(1-x)}$	0.60	0.3302 ± 0.0003	−16.53		−0.25
1061 1	$Co_{(x)}Pd_{(1-x)}$	0.35	0.3835 ± 0.0004	−16.84	−17.13	+0.29
1061 8	$Co_{(x)}Pd_{(1-x)}$	0.60	0.3837 ± 0.0005	−16.84	(QFM)	+0.29
1061 4	$[Ni_{(x)}Mn_{(1-x)}]O$	0.20	n.d.			
1061 6	$[Ni_{(x)}Mn_{(1-x)}]O$	0.09	0.2462 ± 0.0101	−16.77		+0.36
1061 5	$[Ni_{(x)}Mn_{(1-x)}]O$	0.04	0.0521 ± 0.0014	−17.69	−17.70	+0.01
1061 7	$[Ni_{(x)}Mn_{(1-x)}]O$	0.12	0.0531 ± 0.0010	−17.67	(CCO)	+0.03
1061 10	$[Ni_{(x)}Mn_{(1-x)}]O$	0.20	0.0784 ± 0.0028	−17.40		+0.30

Note: Duration = 108 h, T = 700 °C, P = 2.0 kbar.

drolytic weakening of quartz (Ord and Hobbs, 1986). The strength of quartz has been shown to decrease strongly with increasing f_{H_2}. Such experiments highlight the need for simple and accurate methods for monitoring ambient redox conditions in a range of experimental devices.

In the laboratory, the experimental system may be buffered by the oxidation of the walls of the pressure vessel reacting with the gas-fluid pressure medium or alternatively by degassing and dehydration of the furnace assembly in solid-media high-pressure apparatus. Popp et al. (1984) used the Ag-AgCl H sensor to investigate f_{H_2} in rapid-quench hydrothermal vessels. They found that f_{H_2} varied from around NNO when H_2O was used as the pressure-transmitting medium to much lower (~HM) when Ar was used. Unfortunately there has been no comparable study in solid-media high-pressure apparatus, for which there would be a number of advantages in knowing how f_{H_2} varies as a function of time, P, and T. Such information could extend the life of solid buffer assemblages, and, in experiments where the use of an external buffer capsule is difficult (e.g., because of size constraints or when thermal gradients are to be minimized), detailed knowledge of f_{H_2} in the assembly will permit experiments to be performed unbuffered. The use of redox sensors to gather this information would have a distinct advantage over other f_{H_2} sensing techniques since they are easily scaled down for use in confined space, require no complex microchemical analysis, and can give a precise measure of f_{O_2}.

In experimental equipment with accurate f_{H_2} constraint but poor temperature control (e.g., piston-cylinder apparatus with outer solid-buffer capsule), the sensors could also be used as accurate geothermometers.

Mass transfer and osmotic equilibrium

The experiments described herein require H pressure equilibration across the sensor charge walls, and thus H_2 flow rates through semipermeable metal membranes could be accurately monitored by extent of reaction calculations. Triple-capsule techniques are required, where an innermost crimped but unsealed sensor charge is placed within a solid O buffer contained in an hermetically sealed, H-permeable capsule. This twin-charge configuration should be placed within a welded, essentially H-impermeable outer charge containing a different O buffer. Small masses of sensor exposed to this static H_2 pressure gradient for a range of experimental durations at constant T and P would provide accurate, easily retrieved, reversed data on H diffusion rates.

This method is an adaptation of an investigation by Chou (1986) using the Ag-AgCl H sensor as the innermost capsule. In his study, Chou measured H flow across the sealed Ag-AgCl sensor capsule by weight-change calculations. This method is subject to the potentially large errors associated with charge-buffer alloying and material loss during extraction and puncturing. The solid H sensors would overcome these complications.

Determination of mixing properties in solid solutions

Just as Chou (1978) used the Ag-AgCl f_{H_2} sensor to provide an internally consistent set of data for various f_{O_2} buffers, the binary solid solutions may be employed as high-pressure free-energy indicators for many O-dependent equilibria. The accuracy, precision, and analytical simplicity of the solid sensors render them capable of providing the best thermodynamic data available for a vast range of naturally occurring solid-solution assemblages. For example, the activity-composition relations of any mineral containing Fe as a solid-solution component can be determined at any P and T of interest. Using the QFM experiment as an illustration, dilution of the fayalite by addition of a forsterite component will generate more O at fixed P and T than for the pure buffer. The calculated f_{O_2} can be used, with an equation such as Equation 5, to provide activity coefficients for the fayalite component of the olivine solid solution. The O sensor technique has some distinct advantages over the "intrinsic oxygen fugacity" EMF cell (O'Neill, 1987a, 1987b), which has recently provided the best available thermodynamic data for a number of anhydrous phases. Solid solutions equilibrate in a hydrous environment, which dramatically enhances reaction kinetics and permits evaluation of the thermochemical properties of hydrous assemblages. In contrast, the EMF cell operates under low pressures (≈1 bar), and its use is thus restricted to the study of anhydrous compounds. The f_{H_2} sensors can op-

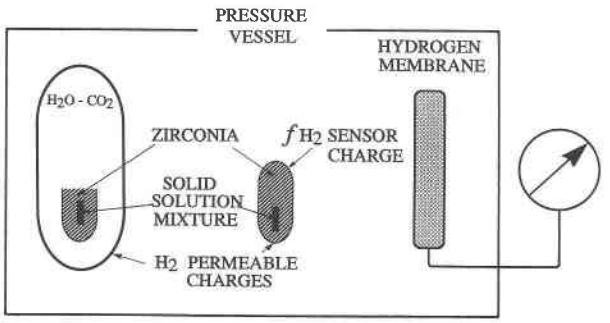

Fig. 8. Experimental design for measurement of H_2O activities in supercritical C-H-O fluids.

erate over a vast range of pressures and temperatures and thus, unlike EMF cells, can be used for the investigation of complex phase transformations.

Measurements of mixing properties in supercritical fluids

All previous discussion has dealt with the effects of diluting one of the solid components in the MMO buffer systems. It is, however, equally plausible to consider the effects on f_{O_2} of reducing the f_{H_2O} of the sensor system by addition of another miscible fluid phase. For the sake of simplicity and geological applicability, let us consider CO_2. If the sensor components are essentially insoluble in H_2O-CO_2 fluid mixtures, then dilution of the pure H_2O fluid with the CO_2 component will reduce the f_{H_2O} in the fluid phase according to Equation 7:

$$\log f_{H_2O}^{mix} = \log f_{H_2} + \frac{1}{2} \log f_{O_2}^{mix} - \log K_{(T,P)}. \quad (7)$$

At constant P, T, and f_{H_2}, the change in f_{O_2} recorded by the redox sensors between a reference capsule containing a pure H_2O fluid phase and another containing a H_2O-CO_2 fluid mixture will enable a direct determination of f_{H_2O} in the fluid mixture. Figure 8 demonstrates one possible experimental procedure for such an investigation. Using this method, preliminary activity-composition data for H_2O-CO_2 binary fluids have been obtained at 700 °C, 2.0 kbar (Pownceby et al., 1990). In this manner, activity-composition relations for numerous binary, H-bearing fluids could be accurately determined over their miscible range.

Other possible sensors

Several other sensors can be designed to accommodate a range of experimental applications. Specific temperature and f_{O_2} range restrictions, experimental apparatus limitations, or charge-wall alloy difficulties could mitigate against the sensor compositions described above. For the NNO-bearing sensors, Cu could be substituted for the more expensive Pd, in the form of an Ni-bearing binary alloy. Co- or Ni-bearing Pt alloys can be used at far higher temperatures, albeit over a more restricted thermal range, than their Pd-bearing equivalents, because of an elevated solidus in the former systems. Similar f_{O_2} may also be surveyed by diluting the metallic component of the iron-wüstite buffer. Fe readily forms alloys with Pt, Pd, and Ir, enabling the buffer to monitor f_{O_2} from IW to around QFM. Caution however must be exercised since (1) many Fe-bearing alloys have a number of a complex phase transitions at $T < 1000$ °C (Massalski, 1986), and (2) any system that surveys more oxidizing conditions will pass through the wüstite-magnetite buffer reaction.

Extending the redox range of sensors, we can select both more oxidized and more reduced metal–metal oxide buffers. The metallic component of the molybdenum–molybdenum oxide buffer can form a continuous solid-solution series with Cr, Nb, or Ti and thereby be successfully driven to more oxidized conditions. At the more oxidized end, it is possible to use the copper–copper oxide buffer ($CuCu_2O$) and the continuous metallic solid solutions formed between Cu and Au, Ni, or Pd. Considerable care should be exercised with the $CuCu_2O$ system, as progression to more oxidizing conditions in the range of this sensor will encounter the Cu_2O-CuO transition. The Mo-bearing alloys only operate at high temperatures (>900 °C), whereas Cu alloys have a narrower range and are limited to lower temperatures by cotectic melting restrictions (<1080 °C).

Once fully calibrated, silicate sensors (e.g., based on QFM) could be extremely useful for high-temperature, long-duration experiments. Such sensors have the advantage of not requiring a zirconia jacket and, in deference to reaction stoichiometry, may be capable of spanning a broader range of f_{O_2}.

Conclusions

Accurate sensors of f_{H_2} in experimental systems have been developed and tested over the P-T range 700–800 °C, 2.0 kbar. The four operating sensor systems can monitor and bracket f_{O_2} over a broad range of T vs. f_{O_2} space ranging from IW to HM. The sensors are reversible, in experimental time frames, down to at least 700 °C and sensitive to about ±0.01 log units f_{O_2}, being limited by analytical precision of the sensor crystalline solutions. The sensor compositions are extremely sensitive to small thermal variations and will only provide an accurate redox measurement in experimental systems with effective temperature control. Inert zirconia jackets permit the sensors to operate within but physically remote from H-permeable, precious-metal capsules.

The lower temperature working range, as well as the absolute accuracy of the sensors, is restricted only by the current reliability of the activity-composition relations in the relevant binary compound systems. Once fully calibrated, the sensors will enable the collection of accurate thermochemical data for redox-sensitive crystalline solutions as well as H-bearing binary fluid mixtures.

Acknowledgments

This research constituted a small part of J.R.T.'s Ph.D. thesis. Financial assistance during this prolonged period of gainful unemployment was pro-

vided by a Commonwealth Postgraduate Research Award and a generous stipend from Aberfoyle Exploration Pty. Ltd. (now Aberfoyle Services P/L). Hugh Skey and Max Richards from Aberfoyle are gratefully acknowledged for their willingness to support the study. Alf Hohmann's technical expertise with the analytical phase was invaluable, and Draga Gelt's artistic assistance was greatly appreciated. Hugh O'Neill's critical review and many helpful suggestions dramatically improved an early, and largely incomprehensible, manuscript. A final vote of thanks to Steven Huebner and Ken Windom for their constructive reviews.

References cited

Aukrust, E., and Muan, A. (1963) Activities of components in oxide solid solutions: The systems CoO-MgO, CoO-MnO, and CoO-"FeO" at 1200 °C. Transactions of the Metallurgical Society of AIME, 227, 1378–1380.

Barret, C.A., and Evans, E.B. (1964) Solid solubility and lattice parameter of NiO-MnO. Journal of the American Ceramic Society, 47, 533.

Bergman, B., and Ågren, J. (1985) Thermodynamic assessment of the system MnO-NiO. Journal of the American Ceramic Society, 68, 444–450.

Bidwell, L.R., and Speiser, R. (1965) The relative thermodynamic properties of solid nickel-palladium alloys. Acta Metallurgica, 13, 61–70.

Brezny, B., and Muan, A. (1971) Activity-composition relations of solid solutions and stabilities of Mg_2TiO_4, $MgTiO_3$ and $MgTi_2O_5$ as determined from equilibria in the system MgO-CoO-TiO_2 at 1300 °C. Thermochimica Acta, 2, 107–119.

Carapezza, M. (1966) A method for continuously variable control of the fugacity of a gas in hydrothermal synthesis at high pressure. Geochemistry International, 3, 819–823.

Chou, I.-M. (1978) Calibration of oxygen buffers at elevated P and T using the hydrogen fugacity sensor. American Mineralogist, 63, 690–703.

——— (1986) Permeability of precious metals to hydrogen at 2 kb total pressure and elevated temperatures. American Journal of Science, 286, 638–658.

Chou, I.-M., and Eugster, H.P. (1976) A sensor for hydrogen fugacities at elevated P and T and applications. Transactions of the American Geophysical Union, 57, 340.

Eugster, H.P. (1957) Heterogeneous reactions involving oxidation and reduction at high temperatures and pressures. Journal of Chemical Physics, 26, 1760–1761.

Eugster, H.P., and Skippen, G.B. (1967) Igneous and metamorphic reactions involving gas equilibria. In P.H. Abelson, Ed., Researches in geochemistry, vol. 2, p. 492–520. Wiley, New York.

Evans, L.G., and Muan, A. (1971) Activity-composition relations of solid solutions and stabilities of end-member compounds in the system MgO-NiO-TiO_2 in contact with metallic nickel at 1400 °C. Thermochimica Acta, 2, 121–134.

Frantz, J.D., and Eugster, H.P. (1973) Acid-base buffers: Use of Ag + AgCl in the experimental control of solution equilibria at elevated pressures and temperatures. American Journal of Science, 273, 268–286.

Gunter, W.D., Myers, J., and Girsperger, S. (1987) Hydrogen: Metal membranes. In G.C. Ulmer and H.L. Barnes, Eds., Hydrothermal experimental techniques, p. 100–120. Wiley, New York.

Hahn, W.C., Jr., and Muan, A. (1961) Activity measurements in oxide solid solutions: The systems NiO-MgO and NiO-MnO in the temperature interval 1100–1300 °C. Journal of Physics and Chemistry of Solids, 19, 338–348.

——— (1970) Activities of the oxide components in NiO-MnO-MgO solid solutions. Materials Research Bulletin, 5, 955–964.

Huebner, J.S. (1971) Buffering techniques for hydrostatic systems at elevated pressures. In G.C. Ulmer, Ed., Research techniques for high pressure and high temperature, p. 123–177. Springer-Verlag, New York.

——— (1987) Use of gas mixtures at low pressure to specify oxygen and other fugacities of furnace atmospheres. In G.C. Ulmer and H.L. Barnes, Eds., Hydrothermal experimental techniques, p. 20–61. Wiley, New York.

Hultgren, R., Desai, P.D., Hawkins, D.T., Gleiser, M., Kelley, K.K., and Wagman, D.D. (1973) Selected values of the thermodynamic properties of binary alloys, p. 1223–1228. American Society of Metals, Metals Park, Ohio.

Labus, S., and Rog, G. (1975) The determination of thermodynamic functions of mixing in the system NiO-MnO by a solid electrolyte cell technique. Annales Societatis Chimicae Polonorum, 49, 339–345.

Luth, R.W., and Boettcher, A.L. (1986) Hydrogen and the melting of silicates. American Mineralogist, 71, 264–276.

Massalski, T.B. (1986) Binary alloy phase diagrams, vols. 1–2. American Society for Metals, Metals Park, Ohio.

Meschter, P.J. (1981) Phase boundary-thermodynamic correlation in binary nickel-transition metal systems. In K. Gokcen, Ed., Chemical metallurgy—phase diagrams and solution properties: A tribute to Carl Hagner, p. 257–272. Transactions of the Metallurgical Society of AIME, Warrendale, Pennsylvania.

Nafziger, R.H., Ulmer, G.C., and Woerman E. (1971) Gaseous buffering for the control of oxygen fugacity at one atmosphere. In G.C. Ulmer, Ed., Research techniques for high pressure and high temperature, p. 9–43. Springer-Verlag, New York.

O'Neill, H.St.C. (1987a) Quartz-fayalite-iron and quartz-fayalite-magnetite equilibria and the free energy of formation of fayalite Fe_2SiO_4 and magnetite Fe_3O_4. American Mineralogist, 72, 67–76.

——— (1987b) Free energies of formation of NiO, CoO, Ni_2SiO_4 and Co_2SiO_4. American Mineralogist, 72, 280–291.

Ord, A., and Hobbs, B.E. (1986) Experimental control of the water-weakening effect in quartz. In B.E. Hobbs and H.C. Heard, Eds., Mineral and rock deformation: Laboratory studies. The Patterson Volume. American Geophysical Union Geophysical Monograph 36, 51–72.

Paulsson, H. (1982) Activities of NiO in (Ni,Mg)O solid solutions. Chemica Scripta, 19, 116–117.

Paulsson, H., and Rosén, E. (1977) Thermodynamic studies of high temperature equilibria XVIII. Solid state EMF determinations of NiO activities in (Ni,Mn)O solid solutions. Chemica Scripta, 11, 204–207.

Popp, R.K., Nagy, K.L., and Hajash, A., Jr. (1984) Semiquantitative control of hydrogen fugacity in rapid-quench hydrothermal vessels. American Mineralogist, 69, 557–562.

Pownceby, M.I., Wall, V.J., and Taylor, J.R. (1990) Redox sensors and the derivation of mixing relations in H_2O-CO_2 fluids. Terra Abstracts, 2, 28.

Rigaud, M., Giovannetti, G., and Hone, M. (1974) Determination of the thermodynamic properties of solid solutions of CoO and MgO by a solid-electrolyte galvanic cell in the temperature range 1273 to 1473 K. Journal of Chemical Thermodynamics, 6, 993–998.

Schwerdtfeger, K., and Muan, A. (1965) Activity measurements in Pt-Ni, Pd-Ni, and Pd-Co alloys at 1000 and 1200 °C. Acta Metallurgica, 13, 509–515.

Seetharaman, S., and Abraham, K.P. (1971) Activity measurements in CoO-MgO solid solutions by the solid-state galvanic cell technique. Journal of the Electrochemical Society of India, 20, 54–57.

Seifert, S., and O'Neill, H.St.C. (1987) Experimental determination of actvity-composition relations in Ni_2SiO_4-Mg_2SiO_4 and Co_2SiO_4-Mg_2SiO_4 solid solutions at 1200 K and 0.1 KPa and 1573 K and 0.5 GPa. Geochimica et Cosmochimica Acta, 51, 97–104.

Shaw, H.R. (1963) Hydrogen-water vapour mixtures: Control of hydrothermal atmospheres by hydrogen osmosis. Science, 139, 1220–1222.

Taylor, J.R.P. (1988) Experimental studies on tin in magmatic-hydrothermal systems. Unpublished Ph.D. thesis, Monash University, Clayton, Victoria, Australia.

Torkar, K., and Inselbacher, W. (1980) Thermodynamische untersuchungen am system CoO-MgO. Journal of Solid State Chemistry, 34, 91–95.

Wise, E.M. (1968) Palladium: Recovery, properties, and uses. Academic Press, New York.

Wood, J.R., Chou, I.-M., and Gunter, W.D. (1975) Thermodynamics of supercritical brines; some new experimental techniques. Geological Society of America, Abstracts with Programs, 7, 1321.

Manuscript received November 5, 1990
Manuscript accepted October 25, 1991